

# *Have greenhouse gases intensified the contrast between wet and dry regions?*

Article

Accepted Version

article

Polson, D., Hegerl, G. C., Allan, R. ORCID:  
<https://orcid.org/0000-0003-0264-9447> and Balan Sarojini, B.  
(2013) Have greenhouse gases intensified the contrast  
between wet and dry regions? *Geophysical Research Letters*,  
40 (17). pp. 4783-4787. ISSN 0094-8276 doi:  
10.1002/grl.50923 Available at  
<https://centaur.reading.ac.uk/34442/>

It is advisable to refer to the publisher's version if you intend to cite from the work. See [Guidance on citing](#).

Published version at: <http://dx.doi.org/10.1002/grl.50923>

To link to this article DOI: <http://dx.doi.org/10.1002/grl.50923>

Publisher: American Geophysical Union

All outputs in CentAUR are protected by Intellectual Property Rights law, including copyright law. Copyright and IPR is retained by the creators or other copyright holders. Terms and conditions for use of this material are defined in the [End User Agreement](#).

[www.reading.ac.uk/centaur](http://www.reading.ac.uk/centaur)

**CentAUR**

Central Archive at the University of Reading

Reading's research outputs online

# Auxiliary material for:

## Have greenhouse gases intensified the contrast between wet and dry regions?

### Geophysical Research Letters

*D. Polson, G.C. Hegerl, R.P. Allan, and B. Balan Sarojini*

The supplementary material shows results from the main paper for seasons not included there, results for land only and ocean only and illustrates the robustness of the results to the removal of ENSO, the observational dataset, method of defining the wet and dry regions and results for the wet and dry regions separately. It also provides some background technical details on the removal of the influence of ENSO from the observational precipitation data and choice of seasons.

#### *a. Annual cycle of observed precipitation and influence of ENSO*

Figure S1(a) shows the monthly tropical precipitation averaged over all years for the GPCP dataset in the Northern and Southern Hemispheres. The seasons January, February and March (JFM), April, May June (AMJ), July, August and September (JAS) and October, November and December (OND) where chosen to capture the wettest and driest seasons in each hemisphere. Figure S1(b) shows the HadCRUT4 annual global mean near surface temperature anomalies during the observation period (Morice et al. 2012).

As the record is short, trends will be influenced by ENSO. The influence of ENSO is removed from the observations in each gridbox by regressing the detrended MEI index (Wolter and Timlin 2011) onto detrended precipitation and subtracting the influence of ENSO from the observations in gridboxes where its influence was found to be significant (i.e. p-value

$\leq 0.05$ ) using the Mann-Whitney test (*Kenyon and Hegerl* 2010). Averaging across the simulations should largely remove the influence of ENSO in the multi-model mean as ENSO events occur at random times in the simulations.

Figure S2 shows the timeseries for the Northern and Southern Hemisphere tropical and subtropical dry and wet region precipitation without removing the influence of ENSO, while Figure S3 shows the timeseries with the influence of ENSO removed. To ensure OND is consistent with JFM, the OND data is from the previous year is 1987 to 2009. *Gu et al.* (2007) show that the impact of volcanoes and ENSO on precipitation can be compounded. To distinguish the two, the removal of ENSO was repeated with the years 1991, 1992 and 1993 (defined as volcanic years by *Gu et al.* (2007)) excluded from the regression of ENSO onto the observations. The precipitation changes were not sensitive to treating the volcanic years separately.

#### *b. Observed and modeled dry and wet regions*

Figures S4 and S5 show the locations of the GPCP dry and wet regions respectively, when defined using method 1. Figures S6 and S7 show the locations of the GPCP dry and wet regions when defined using method 2, which allows the size of the regions to change over time. One change worth noting, is the dry regions tending to occur more often over the NH eastern Pacific in the last 10 years of observations. This is consistent with studies showing an intensification of the Walker circulation in the tropical Pacific in recent decades (*Merrifield* 2011; *Sohn et al.* 2013).

Figures S8 and S9 show ALL forced simulations dry and wet regions when defined using method 2. The top 4 panels show the percentage of years that each gridbox is defined as a dry region or wet region averaged across all simulations and the bottom 4 panels show the multi-model mean difference between the first 10 years and last 10 years. Figures S10 and S11 shows the same results for RCP4.5 simulations for 2011 to 2035, illustrating that the historical fingerprint results closely resembles a result using a near future fingerprint.

The purpose of examining the wet and dry regions in this way is to determine if they are changing size. Figure S12 shows that in the tropics and subtropics any changes to the size of the dry or wet regions for the GPCP dataset are generally small, ( $<10\%$ ). The ALL forced and RCP4.5 models do not show a consistent change in the size of the dry and wet regions for all simulations while the changes in the multi-model means are small for both ( $<5\%$ ). Changes in the mid-latitudes are somewhat larger for both the observations and the models, however, these are still less than the maximum observed year-to-year variation except in the SH mid-latitudes, particularly in JAS where the expansion of the wet regions and reduction of the dry regions is consistent with increasing precipitation at these latitudes.

### *c. Observed and modeled changes in precipitation*

Figures S13 and S14 show the observed and simulated changes in precipitation in the dry and wet regions for land only and ocean only respectively. Comparison of the figures shows that the pattern of dry gets drier, wet gets wetter in the tropics and subtropics is more consistent over ocean than land.

Long term trends in satellite data are still considered uncertain. To explore data uncertainty to some extent, we compare changes over land with two station-based observational datasets, GPCC and CRU, where both are masked to the wet and dry regions of GPCP (Figure S15). The sign of the changes for GPCC and CRU generally match those of GPCP, with GPCC (which is used to calibrate GPCP), more consistent than CRU.

Figure S16 shows the seasonal precipitation for the GPCP, GPCC and CRU datasets for the Northern Hemisphere high latitudes for the years 1988-2010. The timeseries are similar for all three datasets over land, with no large change in precipitation over this period. While this is unsurprising given that in-situ data are used to cross calibrate satellite data (*Adler et al.* 2003), it shows that trends are well constrained by stations.

Figure S17 shows the scaling factors for the combined fingerprint of the wet and dry regions in all seasons for ALL, GHG, RCP4.5 and NAT forcing for the precipitation changes shown in Figures 2, S13 and S14. Figure S18 shows the scaling factors when the influence of ENSO is not removed from the observations, the detection results are the same except for ALL forcing for land+ocean. The results for GHG and RCP4.5 are similar to those of ALL forcing while NAT forcing is not detected (i.e. the 90% confidence interval includes zero). Figure S19 shows the scaling factors for the dry and wet regions separately. For the wet only regions, both GHG and NAT only forcing are detected. Combining the GHG and NAT fingerprints in the 2-signal analysis shows that only GHG forcing is detected when the fingerprint contains both the wet and dry regions. The aerosol affects on precipitation are highly uncertain and there were not enough simulations for anthropogenic only or anthropogenic aerosol only to derive fingerprints with suitably a low signal signal-to-noise ratio.

Figure S20 shows the scaling factors for the control simulations. These show that there is no bias introduced by the method of selecting the dry and wet regions that leads to false detection results.

## REFERENCES

- Adler, R., et al. (2003), The version 2 global precipitation climatology project (gpcp) monthly precipitation analysis (1979-present), *J. Hydrometeor.*, 4, 1147–1167.
- Gu, G., R. F. Adler, G. J. Huffman, and S. Curtis (2007), Tropical rainfall variability on interannual-to-interdecadal and longer time scales derived from the gpcp monthly product, *J. Climate*, 20(15), 4033–4046, doi:10.1175/JCLI4227.1.

- 99 Kenyon, J., and G. Hegerl (2010), Influence of modes of climate variability on global precip-  
100 itation extremes., *J. Clim.*, *23*, 6248–6262.
- 101 Merrifield, M. A. (2011), A shift in western tropical pacific sea level trends during the 1990s,  
102 *J. Clim.*, *24*(15), 4126–4138.
- 103 Morice, C.P., J.J. Kennedy, N.A. Rayner, and P.D. Jones, 2012: Quantifying uncertainties  
104 in global and regional temperature change using an ensemble of observational estimates:  
105 the HadCRUT4 dataset. *J. Geophys. Res.*, *117*, D08101, doi:10.1029/2011JD017187.
- 106 Sohn, B., S.-W. Yeh, J. Schmetz, and H.-J. Song (2013), Observational evidences of walker  
107 circulation change over the last 30years contrasting with gcm results, *Clim. Dyn.*, *40*(7-8),  
108 1721–1732.
- 109 Wolter, K., and M. S. Timlin (2011), El Nino/Southern Oscillation behaviour since 1871  
110 as diagnosed in an extended multivariate ENSO index (MEI.ext)., *Intl. J. Climatol.*, *31*,  
111 1074–1087.

# 112 **List of Tables**

<small>113</small>	1	List of modelling groups and models used in this analysis	7
--------------------	---	---	---



TABLE 1. List of modelling groups and models used in this analysis

<i>InstituteID</i>	<i>ModelName</i>	<i>Forcing(no.ofsims)</i>
CCCMA	CanESM2	GHG(5), NAT(5),CNT(2), RCP4.5(5)
CNRM-CERFACS	CNRM-CM5	ALL(5), GHG(5), NAT(5), CNT(1)
NASA GISS	GISS-E2-H	ALL(5), GHG(5), NAT(5), CNT(2)
NASA GISS	GISS-E2-R	ALL(5), GHG(5), NAT(5), CNT(2), RCP4.5(3)
MOHC	HadGEM2-ES	GHG(4), NAT(4), CNT(1), RCP4.5(3)
INM	INM-CM4	CNT(1), RCP4.5(1)
IPSL	IPSL-CM5A-LR	GHG(3), NAT(3), CNT(1)
NCC	NorESM1-M	ALL(3), GHG(1), NAT(1), CNT(1), RCP4.5(1)
CSIRO-QCCCE	CSIRO-Mk3.6.0	GHG(5), NAT(5), CNT(1), RCP4.5(1)
NCAR	CCSM4	RCP4.5(5), CNT(1)
MRI	MRI-CGCM3	ALL(5), RCP4.5(1)
EC-EARTH	EC-EARTH	ALL(4)
MIROC	MIROC5	ALL(3), RCP4.5(3)
MIROC	MIROC-ESM	RCP4.5(1)
MIROC	MIROC-ESM-CHEM	RCP4.5(1)
MIROC	MIROC4H	RCP4.5(3)
MPI-M	MPI-ESM-LR	RCP4.5(3)

# 114 List of Figures

115	S1	(a) GPCP monthly mean tropical precipitation (mm per day) in the Northern	
116		and Southern Hemispheres averaged over years 1988-2010. (b) HadCRUT4	
117		annual global mean near surface temperature anomalies (w.r.t. 1961-1990)	
118		(Morice et al. 2012).	14
119	S2	GPCP seasonal precipitation for the years 1988-2010 for the dry and wet	
120		regions in the tropics and subtropics. To ensure that the OND and JFM	
121		seasons are consistent, OND is taken from the previous year (i.e. 1987-2009).	15
122	S3	As Figure S2 but with the influence of ENSO removed.	16
123	S4	As Figure 1 in the body of paper but for all seasons. GPCP dry regions for	
124		OND, JFM, AMJ and JAS for 1988 to 2010 using method 1 (OND is 1987-	
125		2009). TOP FOUR PANELS give the percentage of years each grid box is	
126		defined as a dry region. LOWER FOUR PANELS show difference between	
127		first 10 years and last 10 years (i.e. percentage of years wet in 2001-2010	
128		minus 1988-1997), only grid boxes where the change is not zero are plotted.	
129		ENSO is removed from observations.	17
130	S5	As Figure 1 in the body of paper but for wet regions for all seasons. GPCP	
131		wet regions for OND, JFM, AMJ and JAS for 1988 to 2010 using method	
132		1 (OND is 1987-2009). TOP FOUR PANELS give the percentage of years	
133		each grid box is defined as a wet region. LOWER FOUR PANELS show	
134		difference between first 10 years and last 10 years (i.e. percentage of years	
135		wet in 2001-2010 minus 1988-1997), only grid boxes where the change is not	
136		zero are plotted. ENSO is removed from observations.	18

- S6 As Figure 1 in the body of paper but using method 2 for all seasons. GPCP dry regions for OND, JFM, AMJ and JAS for 1988 to 2010 using method 2 (OND is 1987-2009). TOP FOUR PANELS give the percentage of years each grid box is defined as a dry region. LOWER FOUR PANELS show difference between first 10 years and last 10 years (i.e. percentage of years dry in 2001-2010 minus 1988-1997), only grid boxes where the change is not zero are plotted. ENSO is removed from observations. 19
- S7 As Figure 1 in the body of paper but using method 2 for the wet regions for all seasons. GPCP wet regions for OND, JFM, AMJ and JAS for 1988 to 2010 using method 2 (OND is 1987-2009). TOP FOUR PANELS give the percentage of years each grid box is defined as a wet region. LOWER FOUR PANELS show difference between first 10 years and last 10 years (i.e. percentage of years wet in 2001-2010 minus 1988-1997), only grid boxes where the change is not zero are plotted. ENSO is removed from observations. 20
- S8 Shows similar results to Figure 1 in body of the paper for the models. ALL forced models mean dry regions for OND, JFM, AMJ and JAS for 1988 to 2010 using method 2 (OND is 1987-2009). TOP FOUR PANELS give the multi-model mean percentage of years each grid box is defined as a dry region. LOWER FOUR PANELS show difference between first 10 years and last 10 years (i.e. percentage of years dry in 2001-2010 minus 1988-1997) averaged for all simulations, only grid boxes where the change is not zero are plotted. 21

- S9 Shows similar results to Figure 1 in body of the paper for the models. ALL forced models mean wet regions for OND, JFM, AMJ and JAS for 1988 to 2010 using method 2 (OND is 1987-2009). TOP FOUR PANELS give the multi-model mean percentage of years each grid box is defined as a wet region. LOWER FOUR PANELS show difference between first 10 years and last 10 years (i.e. percentage of years wet in 2001-2010 minus 1988-1997) averaged for all simulations, only grid boxes where the change is not zero are plotted. 22
- S10 Shows similar results to Figure 1 in body of the paper for the models. RCP4.5 forced models mean dry regions for OND, JFM, AMJ and JAS for 2011 to 2035 using method 2 (OND is 2010-2034). TOP FOUR PANELS give the multi-model mean percentage of years each grid box is defined as a dry region. LOWER FOUR PANELS show difference between first 10 years and last 10 years (i.e. percentage of years dry in 2026-2035 minus 2011-2020), only grid boxes where the change is not zero are plotted. 23
- S11 Shows similar results to Figure 1 in body of the paper for the models. RCP4.5 forced models mean wet regions for OND, JFM, AMJ and JAS for 2011 to 2035 using method 2 (OND is 2010-2034). TOP FOUR PANELS give the multi-model mean percentage of years each grid box is defined as a wet region. LOWER FOUR PANELS show difference between first 10 years and last 10 years (i.e. percentage of years wet in 2026-2035 minus 2011-2020), only grid boxes where the change is not zero are plotted. 24
- S12 Changing size of size of dry (TOP FOUR PANELS) and wet (LOWER FOUR PANELS) regions using method 2, i.e. mean number of grid boxes for 2001-2010 minus mean number of grid boxes for 1988-1997 (OND uses 1987-2009), as percentage of mean number of grid boxes in all years in the dry/wet regions. ENSO is removed from observations. 25

S13 As Figure 2 in the body of paper but for land only. Observed and modelled zonal mean trends (% per year) in the dry (TOP FOUR PANELS) and wet (LOWER FOUR PANELS) regions over land for 1988 to 2010 (OND is 1987-2009). Note GPCP changes are plotted on a larger scale and the influence of ENSO is removed from observations. The colored bars give the multi-model mean trends for the ALL, GHG and rcp4.5 simulations. The orange shading show where GPCP, ALL and rcp4.5 all give negative trends and the blue shading shows where they give positive trends.

26

S14 As Figure 2 in the body of paper but for ocean only. Observed and modelled zonal mean trends (% per year) in the dry (TOP FOUR PANELS) and wet (LOWER FOUR PANELS) regions over the ocean for 1988 to 2010 (OND is 1987-2009). Note GPCP changes are plotted on a larger scale and the influence of ENSO is removed from observations. The colored bars give the multi-model mean trends for the ALL, GHG and rcp4.5 simulations. The orange shading show where GPCP, ALL and rcp4.5 all give negative trends and the blue shading shows where they give positive trends.

27

S15 As Figure 2 in body of paper for 3 different observational datasets for land only. Robustness of observed changes over land for 1988 to 2010 (OND is 1987-2009). Observed and multi-model mean zonal mean trends (MM) (% per year) in the dry (TOP FOUR PANELS) and wet (LOWER FOUR PANELS) regions over land for the GPCP, GPCC and CRU observations datasets where the GPCC and CRU datasets were masked to match the dry and wet regions in the GPCP dataset. The orange shading shows where the changes for GPCP, GPCC and CRU are all negative and blue were they are all positive. The changes for all land are also shown for all 3 observation datasets ( $GPCP_{al}$ ,  $GPCC_{al}$  and  $CRU_{al}$ ) and for all land+ocean for GPCP ( $GPCP_{alo}$ ). This influence of ENSO is removed from observations.

28

211 S16 Observed land precipitation in the Northern Hemisphere high latitudes (60N  
212 to 90N) for 1988 to 2010 (OND is 1987-2009) for 3 observational datasets,  
213 GPCP, GPCC and CRU and ocean for GPCP. 29

214 S17 Detection and attribution results: As Figure 3 upper panel but using fin-  
215 gerprints for individual forcings. Scaling factors for the wet and dry regions  
216 combined for ALL, GHG, NAT and RCP4.5 simulations with ENSO removed  
217 from observations Crosses show the 'best-guess' scaling factor for the multi-  
218 model mean, thick lines are the 90% confidence interval for the raw model  
219 variance added as noise and thin lines are the 90% confidence interval for  
220 double the variance. L+O is land+ocean for the GPCP dataset. Note differ-  
221 ent scale used for NAT forcing. The residual consistency test is passed for all  
222 forcings for double the model variance. 30

223 S18 Detection and attribution results: As Figure 3 upper panel and Figure S17  
224 using fingerprints for individual forcings but with ENSO not removed from  
225 observations. Scaling factors for the wet and dry regions combined for ALL,  
226 GHG, NAT and RCP4.5 simulations. Crosses show the 'best-guess' scaling  
227 factor for the multi-model mean, thick lines are the 90% confidence interval for  
228 the raw model variance added as noise and thin lines are the 90% confidence  
229 interval for double the variance. L+O is land+ocean for the GPCP dataset.  
230 Note different scale used for NAT forcing. The residual consistency test is  
231 passed for all forcings for double the model variance. 31

S19 Detection and attribution results: As Figure 3 upper panel but using fingerprints for individual forcings and wet and dry regions separately. Scaling factor for the ALL, GHG, NAT, and RCP4.5 simulations for wet and dry regions separately with ENSO removed from observations. Crosses show the 'best-guess' scaling factor for the multi-model mean, thick lines are the 90% confidence interval for the raw model variance added as noise and thin lines are the 90% confidence interval for double the variance. Note different scale used for NAT forcing. The residual consistency test is passed for all forcings for double the model variance.

32

S20 Detection and attribution results: As Figure 3 upper panel but using fingerprints for control only simulations. UPPER PANEL Scaling factors for the control simulations fingerprint for combined dry and wet regions for land+ocean, ocean only and land only for the 3 observations datasets GPCP, GPCC and CRU and LOWER PANEL individual dry and wet regions for land+ocean for the GPCP dataset. This shows that no artificial trends are introduced by the analysis method that produce false detection if forcing.

33

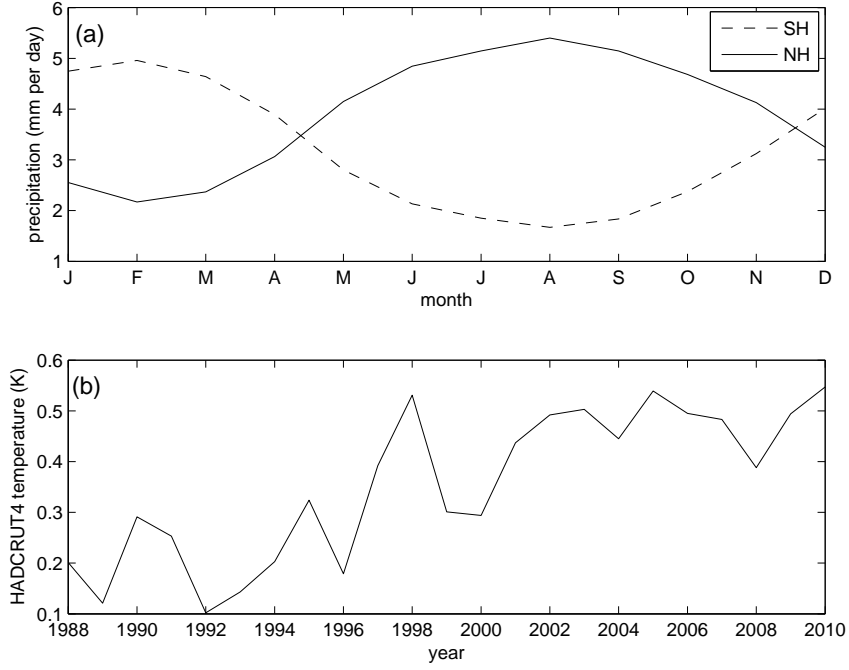


FIG. S1. (a) GPCP monthly mean tropical precipitation (mm per day) in the Northern and Southern Hemispheres averaged over years 1988-2010. (b) HadCRUT4 annual global mean near surface temperature anomalies (w.r.t. 1961-1990) (Morice et al. 2012).



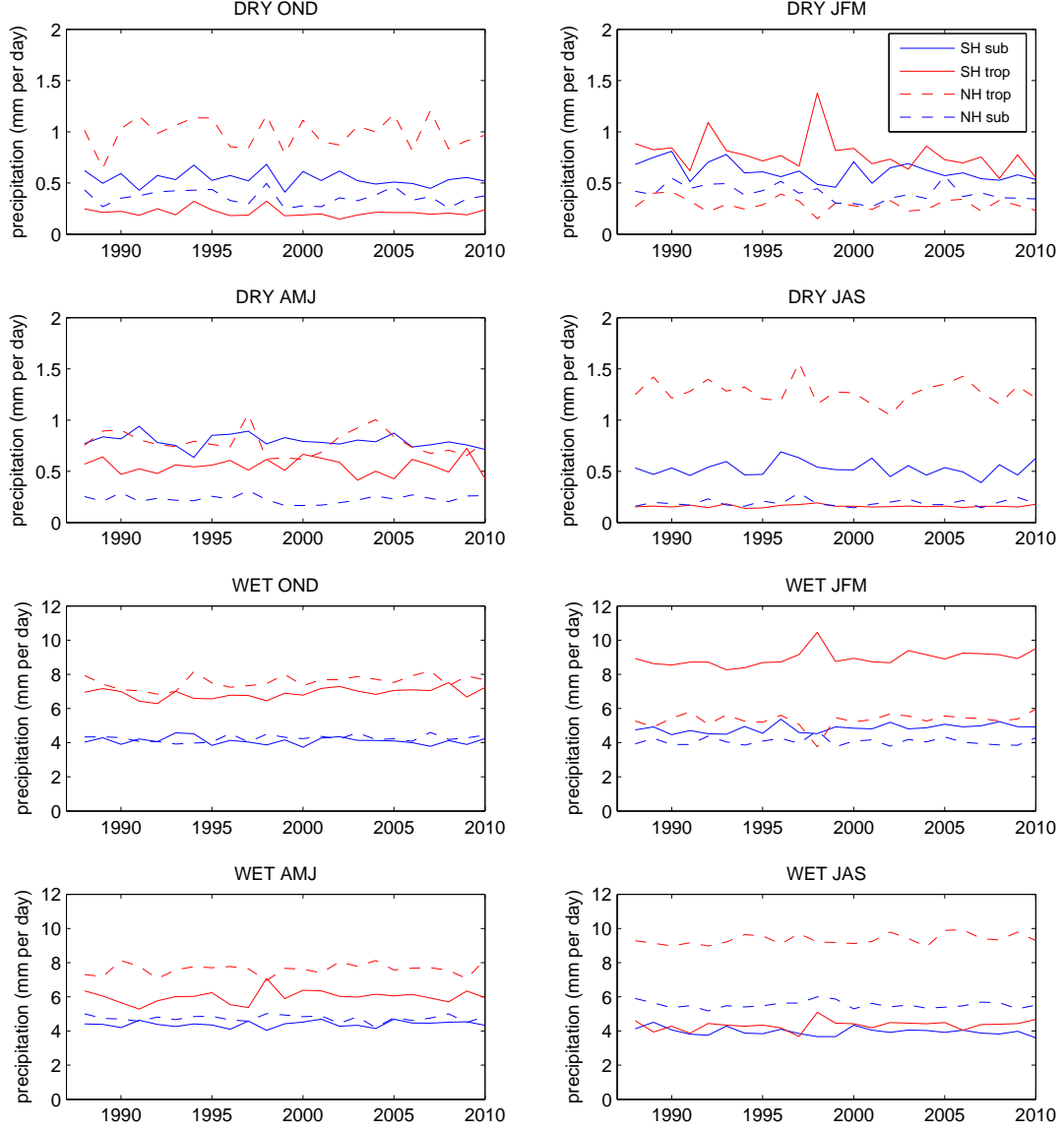


FIG. S2. GPCP seasonal precipitation for the years 1988-2010 for the dry and wet regions in the tropics and subtropics. To ensure that the OND and JFM seasons are consistent, OND is taken from the previous year (i.e. 1987-2009).

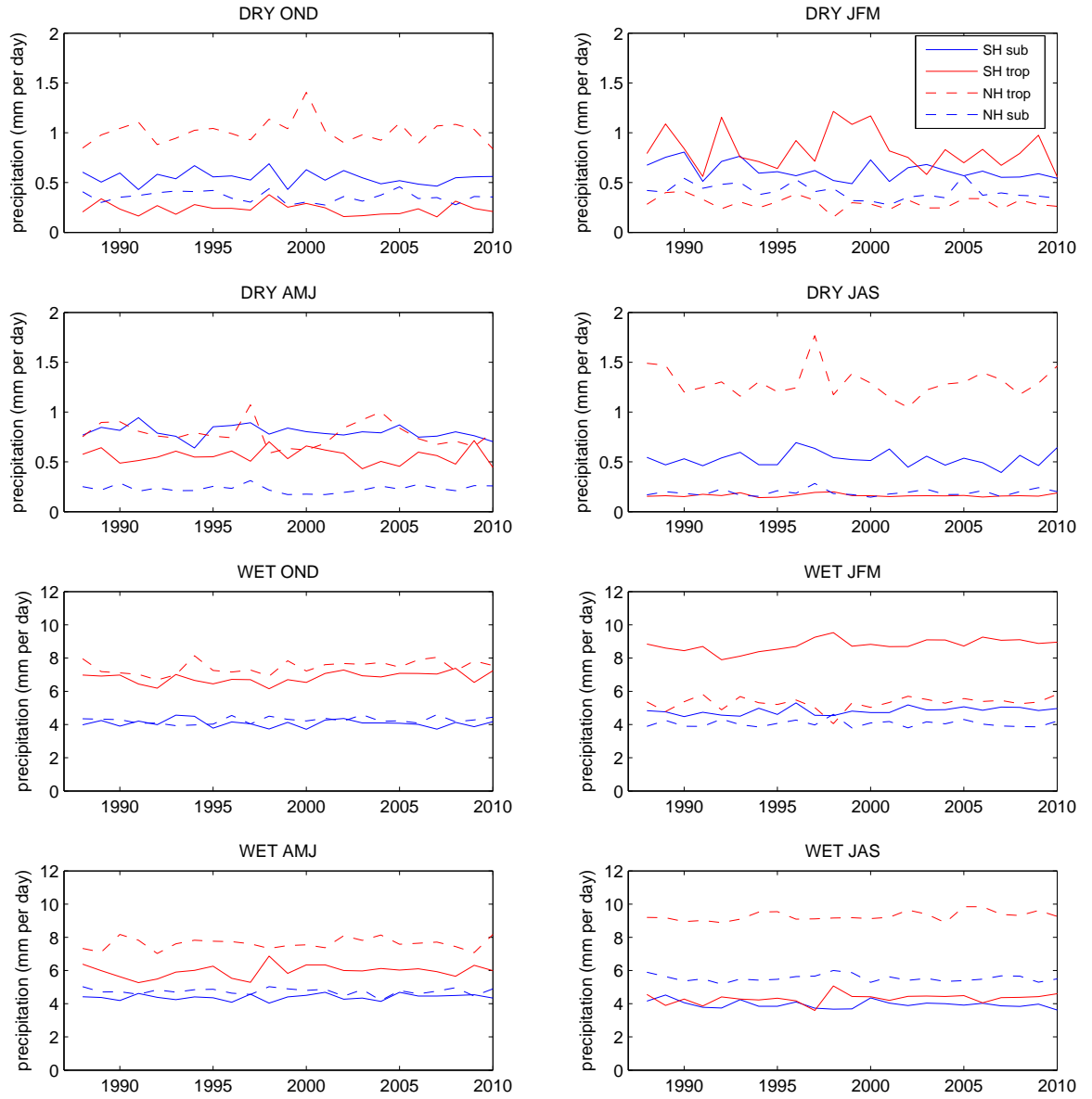


FIG. S3. As Figure S2 but with the influence of ENSO removed.

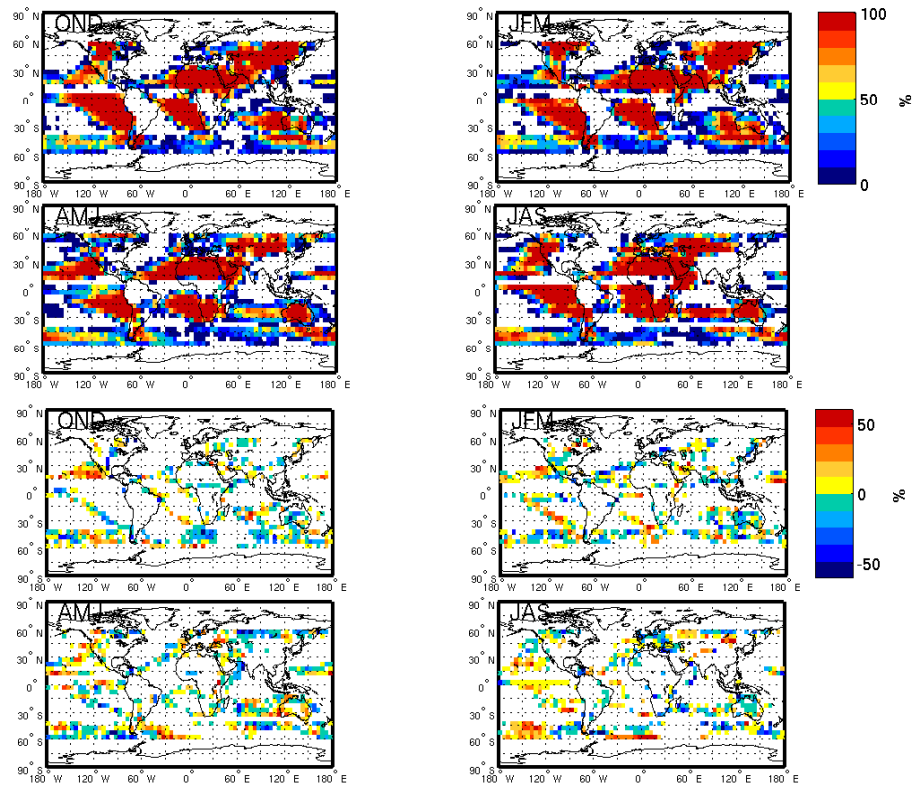


FIG. S4. As Figure 1 in the body of paper but for all seasons. GPCP dry regions for OND, JFM, AMJ and JAS for 1988 to 2010 using method 1 (OND is 1987-2009). TOP FOUR PANELS give the percentage of years each gridbox is defined as a dry region. LOWER FOUR PANELS show difference between first 10 years and last 10 years (i.e. percentage of years wet in 2001-2010 minus 1988-1997), only gridboxes where the change is not zero are plotted. ENSO is removed from observations.

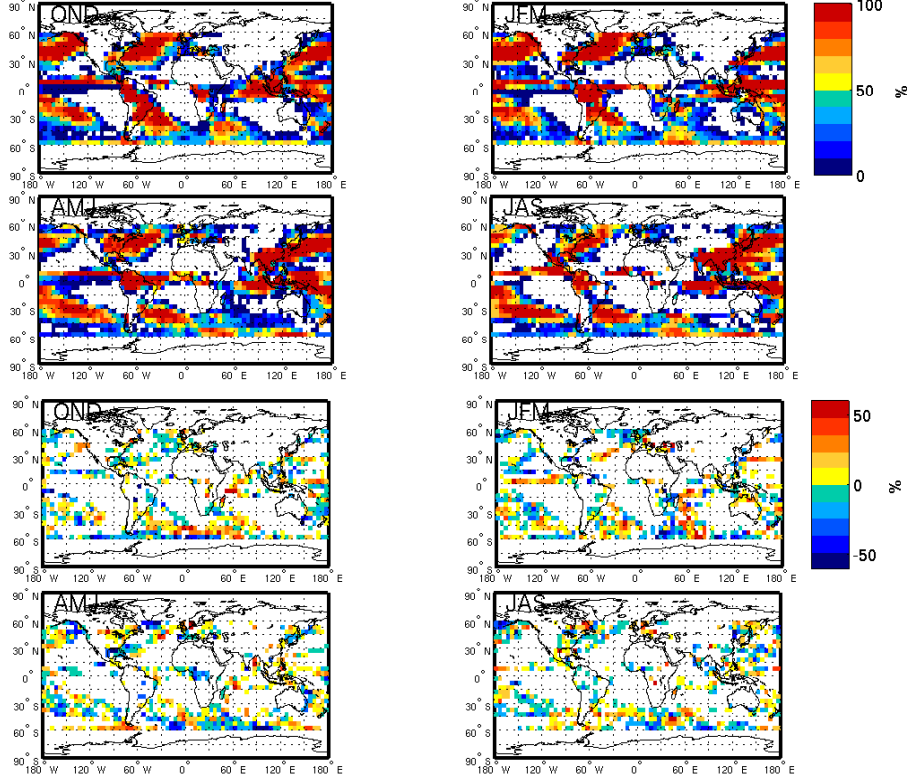


FIG. S5. As Figure 1 in the body of paper but for wet regions for all seasons. GPCP wet regions for OND, JFM, AMJ and JAS for 1988 to 2010 using method 1 (OND is 1987-2009). TOP FOUR PANELS give the percentage of years each gridbox is defined as a wet region. LOWER FOUR PANELS show difference between first 10 years and last 10 years (i.e. percentage of years wet in 2001-2010 minus 1988-1997), only gridboxes where the change is not zero are plotted. ENSO is removed from observations.

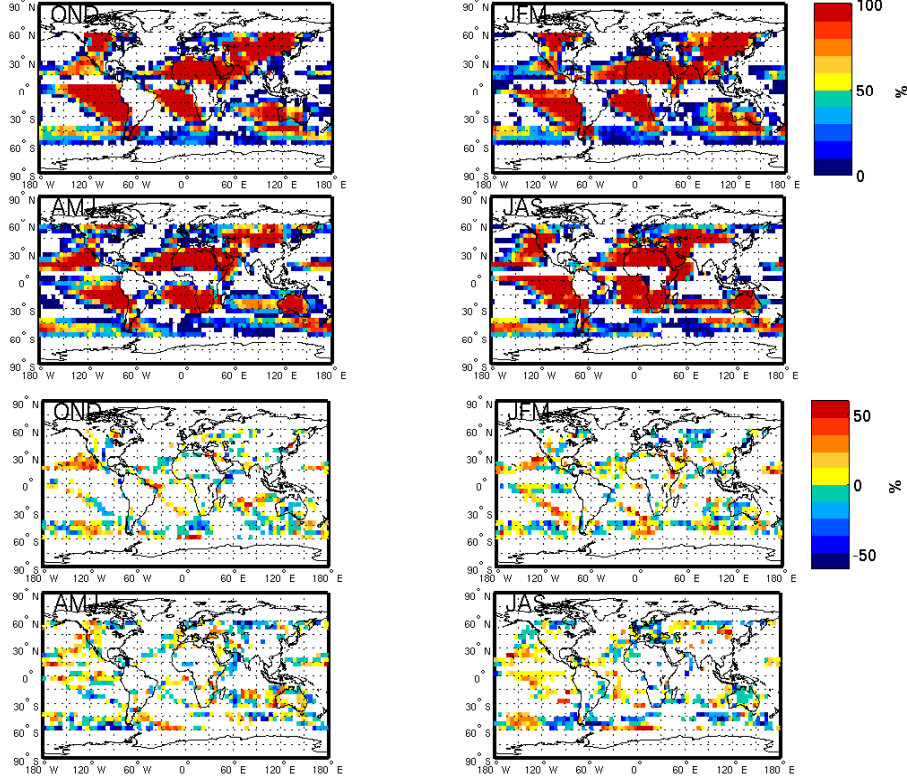


FIG. S6. As Figure 1 in the body of paper but using method 2 for all seasons. GPCP dry regions for OND, JFM, AMJ and JAS for 1988 to 2010 using method 2 (OND is 1987-2009). TOP FOUR PANELS give the percentage of years each gridbox is defined as a dry region. LOWER FOUR PANELS show difference between first 10 years and last 10 years (i.e. percentage of years dry in 2001-2010 minus 1988-1997), only gridboxes where the change is not zero are plotted. ENSO is removed from observations.

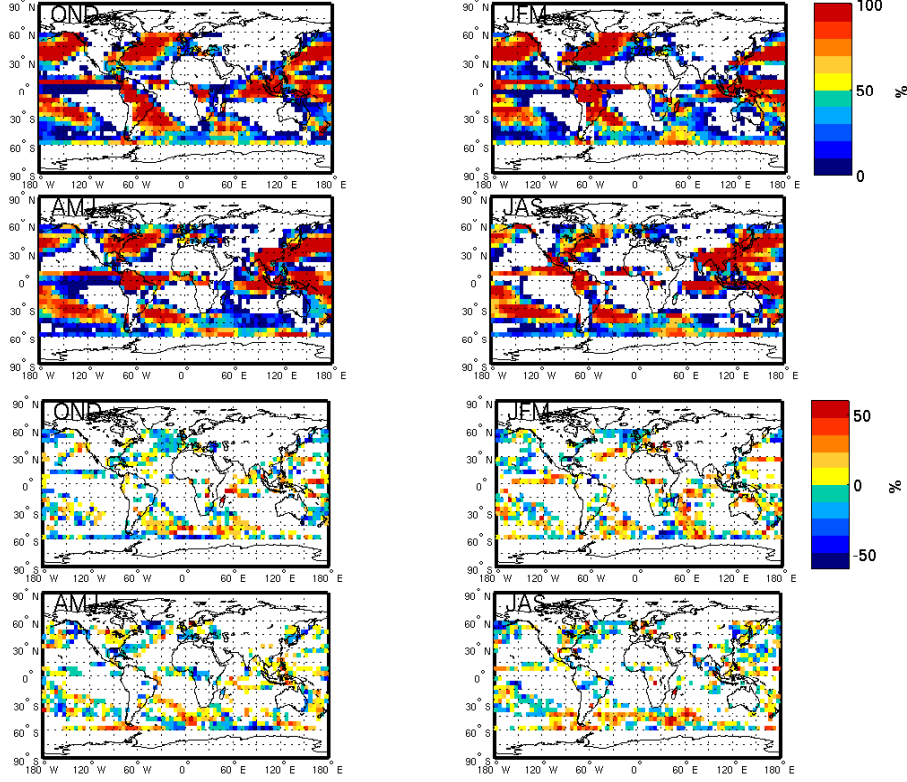


FIG. S7. As Figure 1 in the body of paper but using method 2 for the wet regions for all seasons. GPCP wet regions for OND, JFM, AMJ and JAS for 1988 to 2010 using method 2 (OND is 1987-2009). TOP FOUR PANELS give the percentage of years each gridbox is defined as a wet region. LOWER FOUR PANELS show difference between first 10 years and last 10 years (i.e. percentage of years wet in 2001-2010 minus 1988-1997), only gridboxes where the change is not zero are plotted. ENSO is removed from observations.

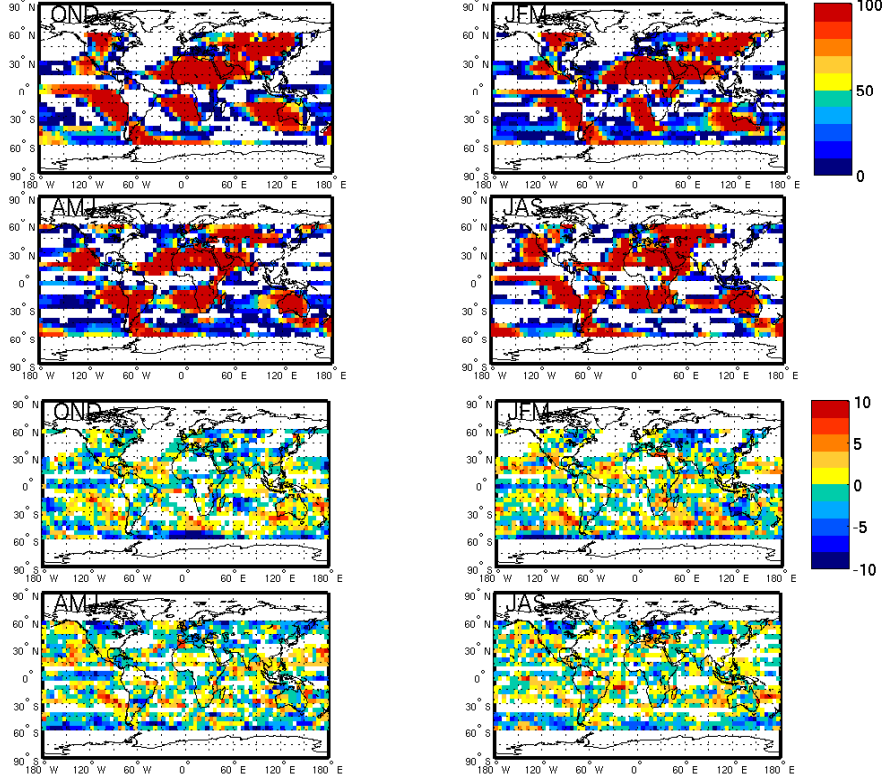


FIG. S8. Shows similar results to Figure 1 in body of the paper for the models. ALL forced models mean dry regions for OND, JFM, AMJ and JAS for 1988 to 2010 using method 2 (OND is 1987-2009). TOP FOUR PANELS give the multi-model mean percentage of years each gridbox is defined as a dry region. LOWER FOUR PANELS show difference between first 10 years and last 10 years (i.e. percentage of years dry in 2001-2010 minus 1988-1997) averaged for all simulations, only gridboxes where the change is not zero are plotted.

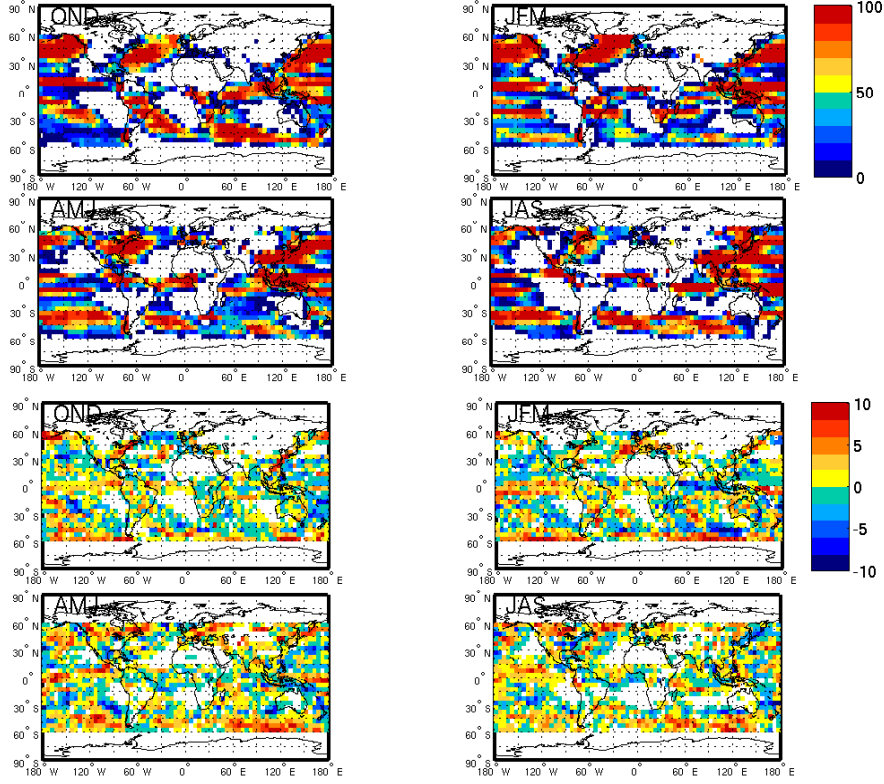


FIG. S9. Shows similar results to Figure 1 in body of the paper for the models. ALL forced models mean wet regions for OND, JFM, AMJ and JAS for 1988 to 2010 using method 2 (OND is 1987-2009). TOP FOUR PANELS give the multi-model mean percentage of years each gridbox is defined as a wet region. LOWER FOUR PANELS show difference between first 10 years and last 10 years (i.e. percentage of years wet in 2001-2010 minus 1988-1997) averaged for all simulations, only gridboxes where the change is not zero are plotted.



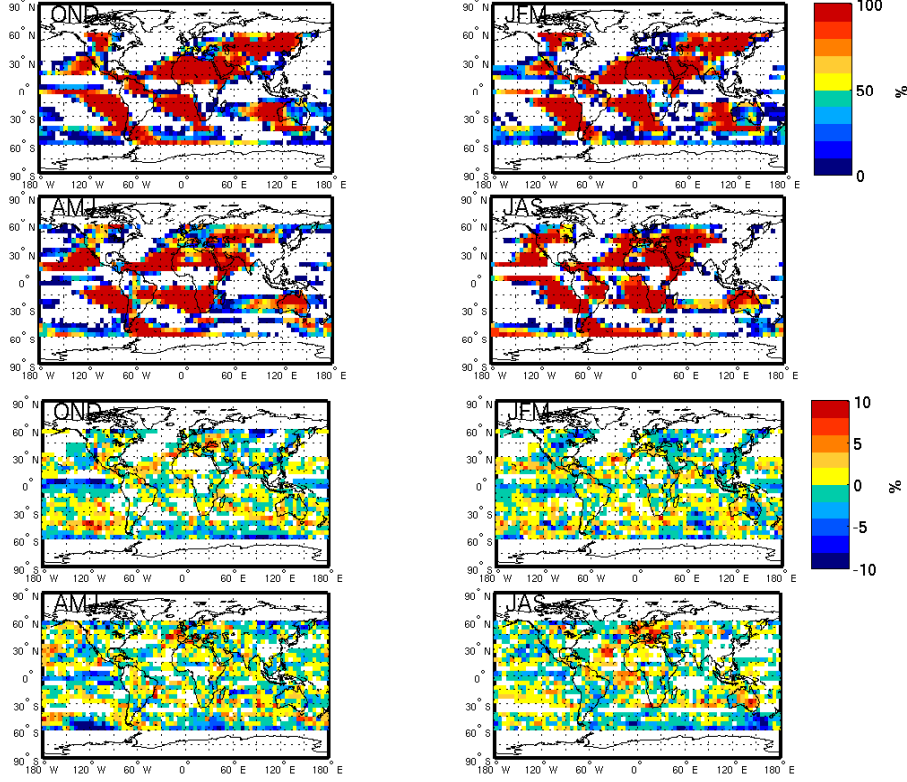


FIG. S10. Shows similar results to Figure 1 in body of the paper for the models. RCP4.5 forced models mean dry regions for OND, JFM, AMJ and JAS for 2011 to 2035 using method 2 (OND is 2010-2034). TOP FOUR PANELS give the multi-model mean percentage of years each gridbox is defined as a dry region. LOWER FOUR PANELS show difference between first 10 years and last 10 years (i.e. percentage of years dry in 2026-2035 minus 2011-2020), only gridboxes where the change is not zero are plotted.

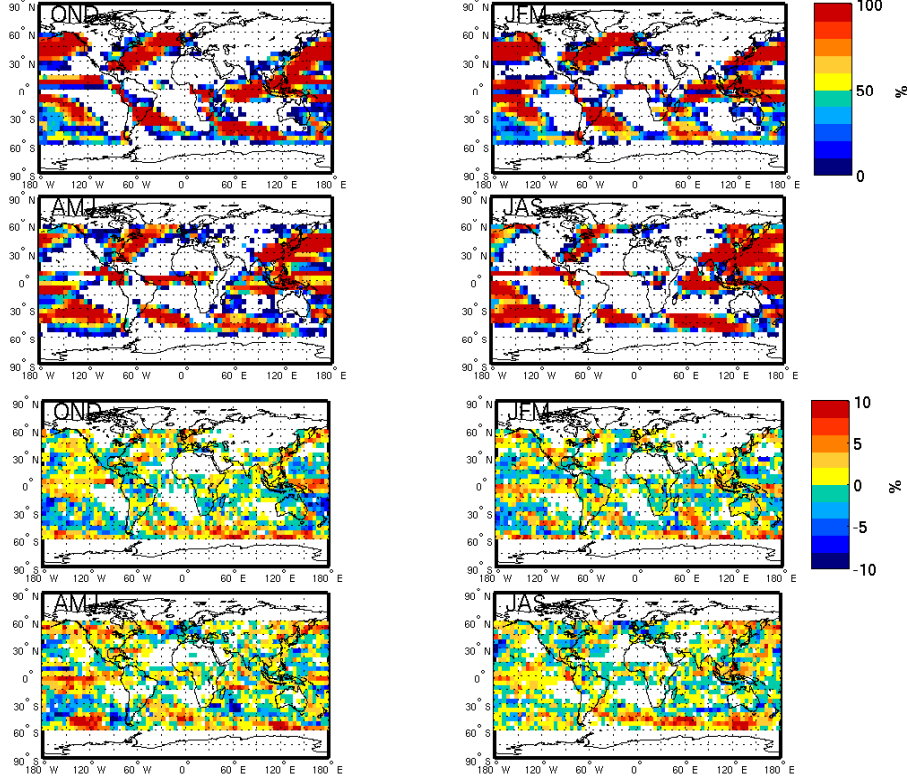


FIG. S11. Shows similar results to Figure 1 in body of the paper for the models. RCP4.5 forced models mean wet regions for OND, JFM, AMJ and JAS for 2011 to 2035 using method 2 (OND is 2010-2034). TOP FOUR PANELS give the multi-model mean percentage of years each gridbox is defined as a wet region. LOWER FOUR PANELS show difference between first 10 years and last 10 years (i.e. percentage of years wet in 2026-2035 minus 2011-2020), only gridboxes where the change is not zero are plotted.

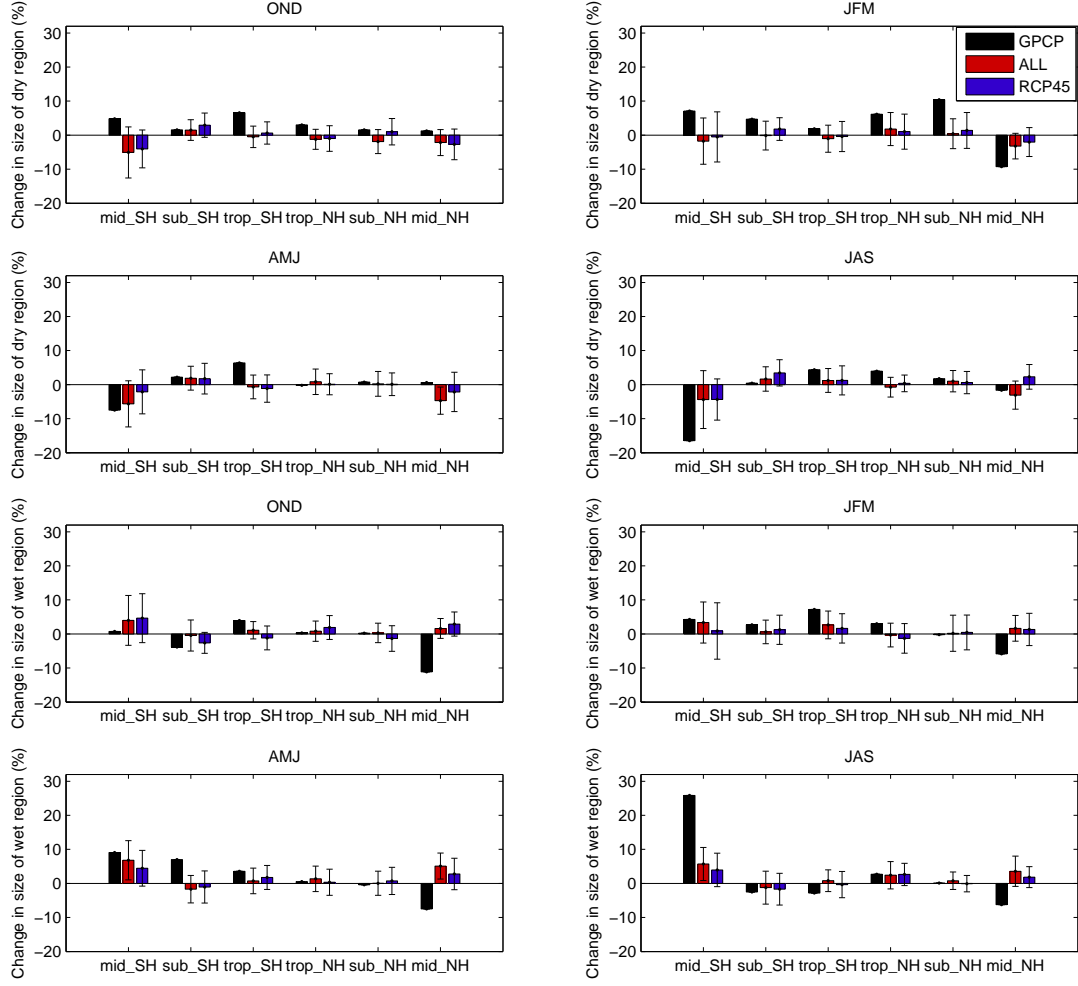


FIG. S12. Changing size of size of dry (TOP FOUR PANELS) and wet (LOWER FOUR PANELS) regions using method 2, i.e. mean number of grid boxes for 2001-2010 minus mean number of gridboxes for 1988-1997 (OND uses 1987-2009), as percentage of mean number of gridboxes in all years in the dry/wet regions. ENSO is removed from observations.

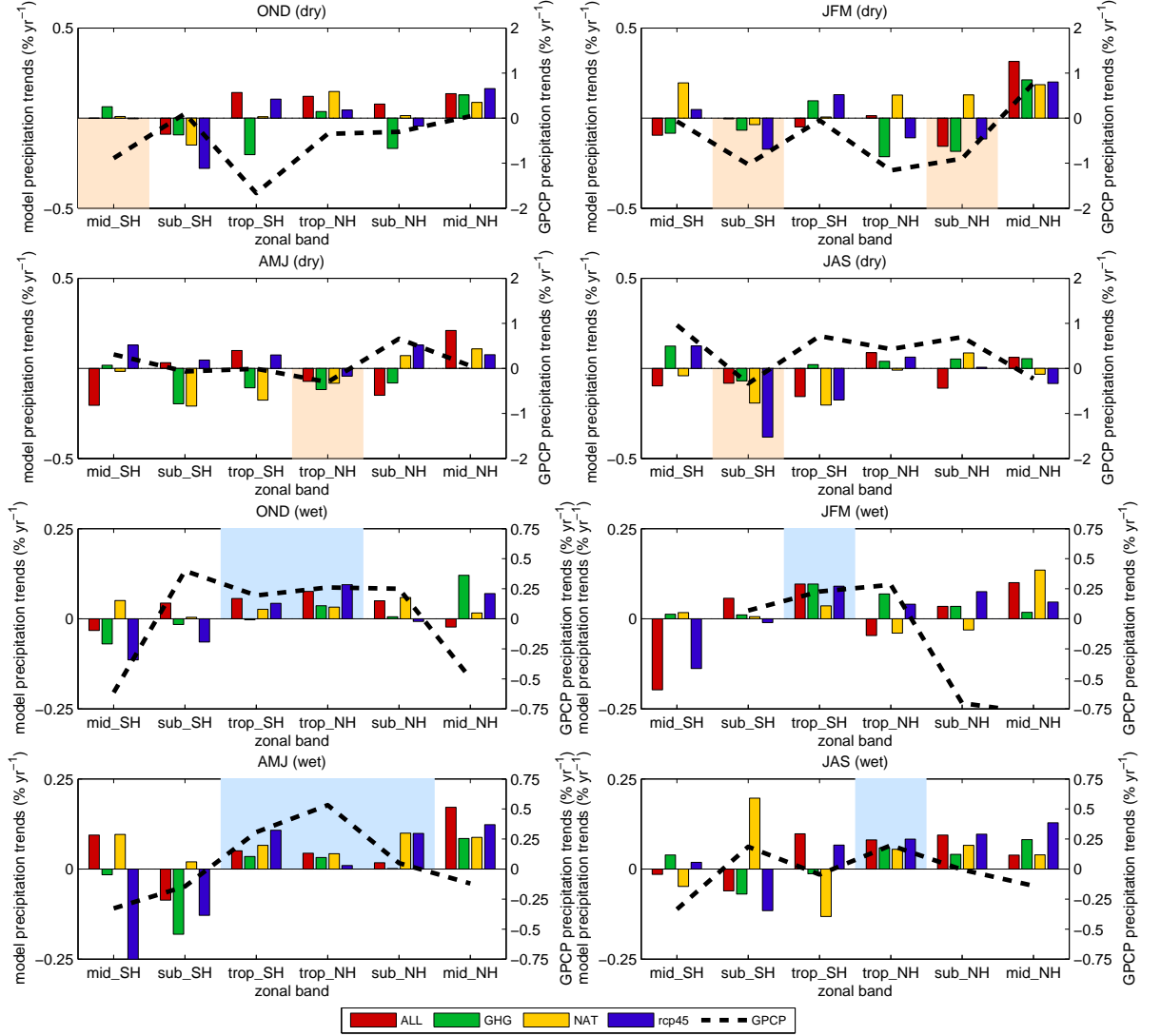


FIG. S13. As Figure 2 in the body of paper but for land only. Observed and modelled zonal mean trends (% per year) in the dry (TOP FOUR PANELS) and wet (LOWER FOUR PANELS) regions over land for 1988 to 2010 (OND is 1987-2009). Note GPCP changes are plotted on a larger scale and the influence of ENSO is removed from observations. The colored bars give the multi-model mean trends for the ALL, GHG and rcp4.5 simulations. The orange shading show where GPCP, ALL and rcp4.5 all give negative trends and the blue shading shows where they give positive trends.

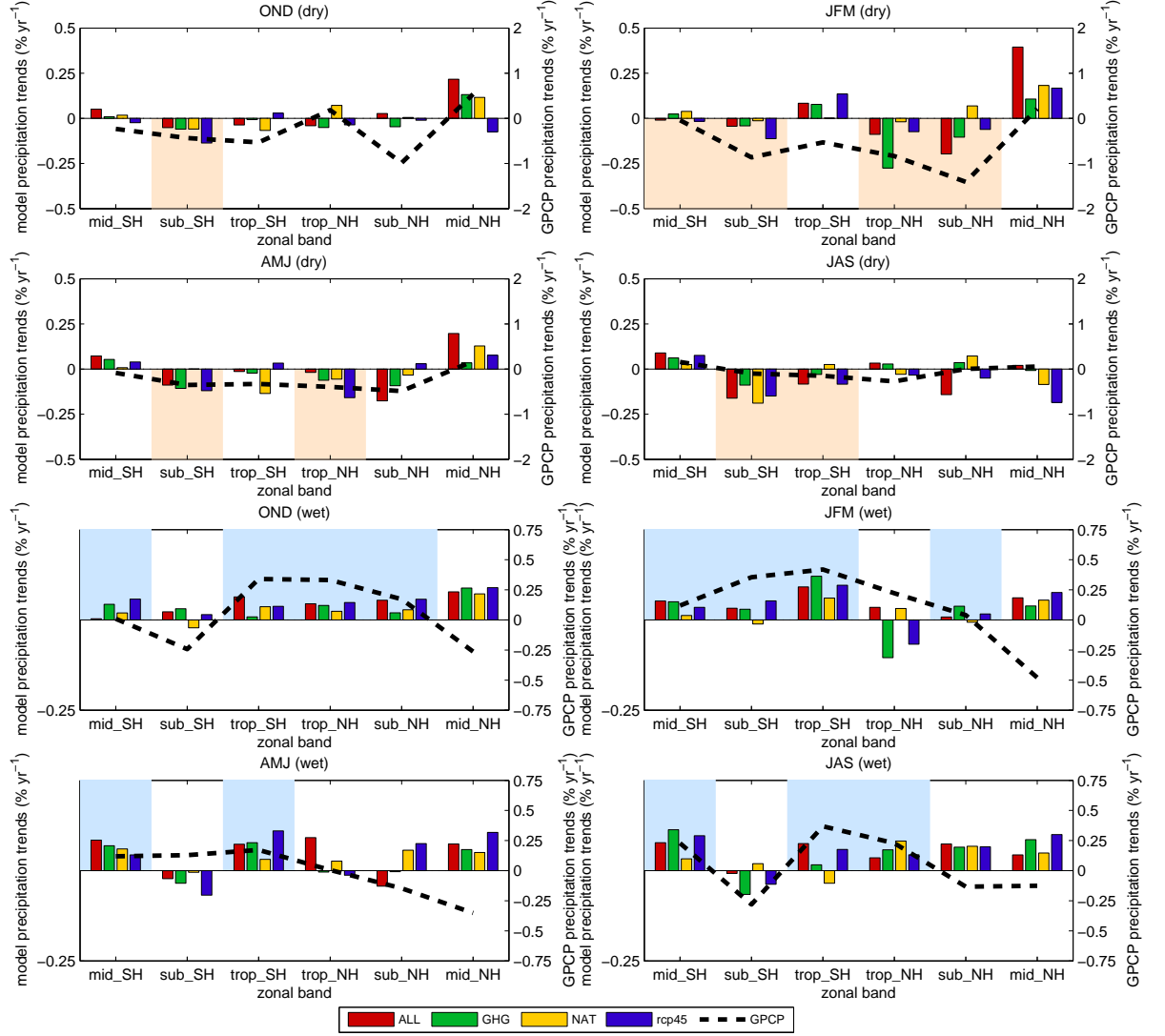


FIG. S14. As Figure 2 in the body of paper but for ocean only. Observed and modelled zonal mean trends (% per year) in the dry (TOP FOUR PANELS) and wet (LOWER FOUR PANELS) regions over the ocean for 1988 to 2010 (OND is 1987-2009). Note GPCP changes are plotted on a larger scale and the influence of ENSO is removed from observations. The colored bars give the multi-model mean trends for the ALL, GHG and rcp4.5 simulations. The orange shading show where GPCP, ALL and rcp4.5 all give negative trends and the blue shading shows where they give positive trends.

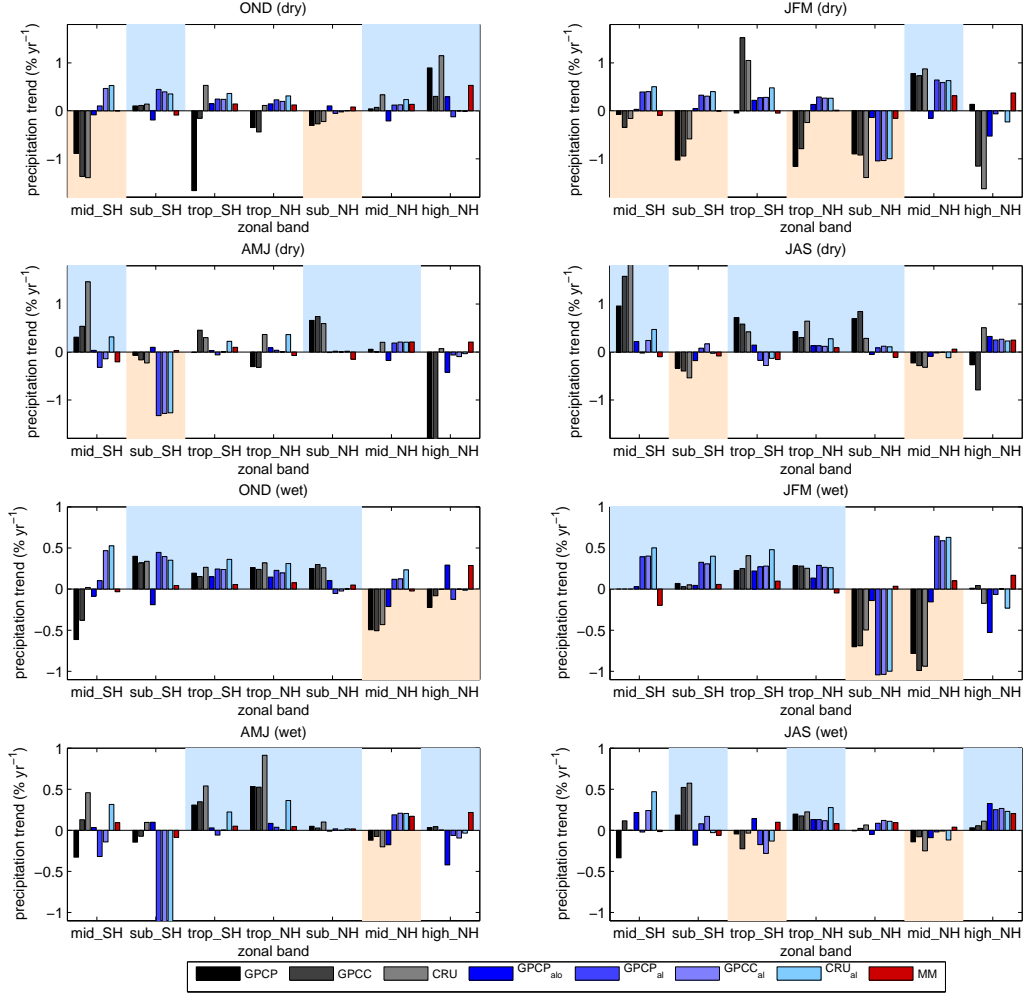


FIG. S15. As Figure 2 in body of paper for 3 different observational datasets for land only. Robustness of observed changes over land for 1988 to 2010 (OND is 1987-2009). Observed and multi-model mean zonal mean trends (MM) (% per year) in the dry (TOP FOUR PANELS) and wet (LOWER FOUR PANELS) regions over land for the GPCP, GPCC and CRU observations datasets where the GPCC and CRU datasets were masked to match the dry and wet regions in the GPCP dataset. The orange shading shows where the changes for GPCP, GPCC and CRU are all negative and blue were they are all positive. The changes for all land are also shown for all 3 observation datasets ( $GPCP_{al}$ ,  $GPCC_{al}$  and  $CRU_{al}$ ) and for all land+ocean for GPCP ( $GPCP_{alo}$ ). This influence of ENSO is removed from observations.

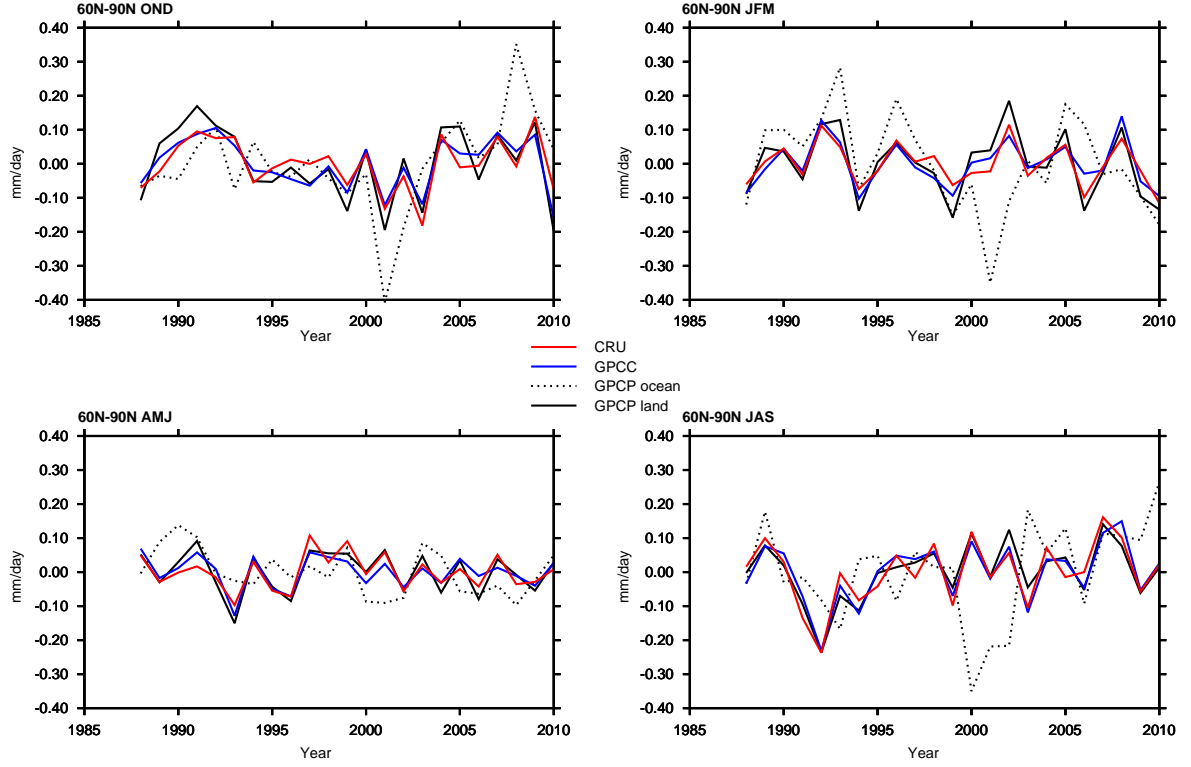


FIG. S16. Observed land precipitation in the Northern Hemisphere high latitudes (60N to 90N) for 1988 to 2010 (OND is 1987-2009) for 3 observational datasets, GPCP, GPCC and CRU and ocean for GPCP.

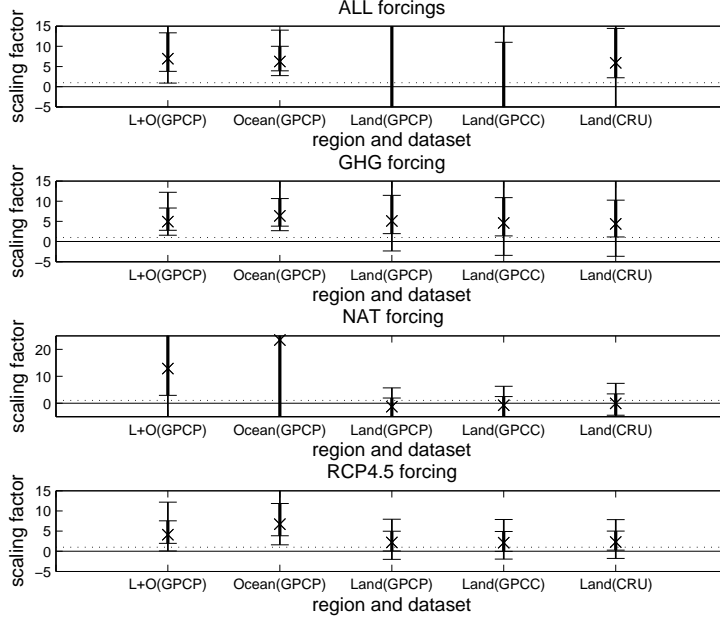


FIG. S17. Detection and attribution results: As Figure 3 upper panel but using fingerprints for individual forcings. Scaling factors for the wet and dry regions combined for ALL, GHG, NAT and RCP4.5 simulations with ENSO removed from observations. Crosses show the 'best-guess' scaling factor for the multi-model mean, thick lines are the 90% confidence interval for the raw model variance added as noise and thin lines are the 90% confidence interval for double the variance. L+O is land+ocean for the GPCP dataset. Note different scale used for NAT forcing. The residual consistency test is passed for all forcings for double the model variance.



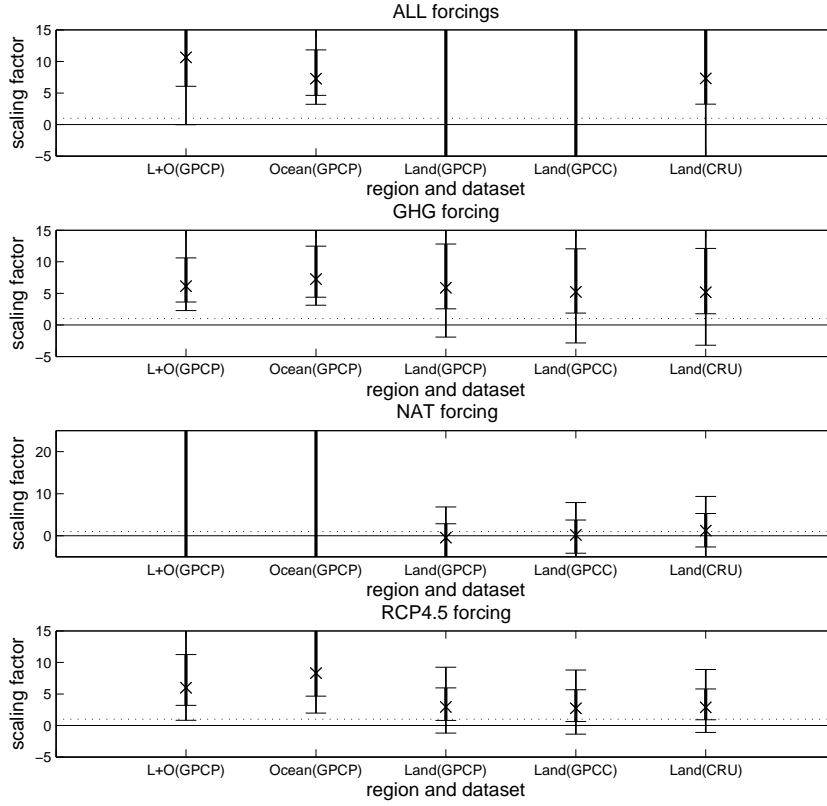


FIG. S18. Detection and attribution results: As Figure 3 upper panel and Figure S17 using fingerprints for individual forcings but with ENSO not removed from observations. Scaling factors for the wet and dry regions combined for ALL, GHG, NAT and RCP4.5 simulations. Crosses show the 'best-guess' scaling factor for the multi-model mean, thick lines are the 90% confidence interval for the raw model variance added as noise and thin lines are the 90% confidence interval for double the variance. L+O is land+ocean for the GPCP dataset. Note different scale used for NAT forcing. The residual consistency test is passed for all forcings for double the model variance.

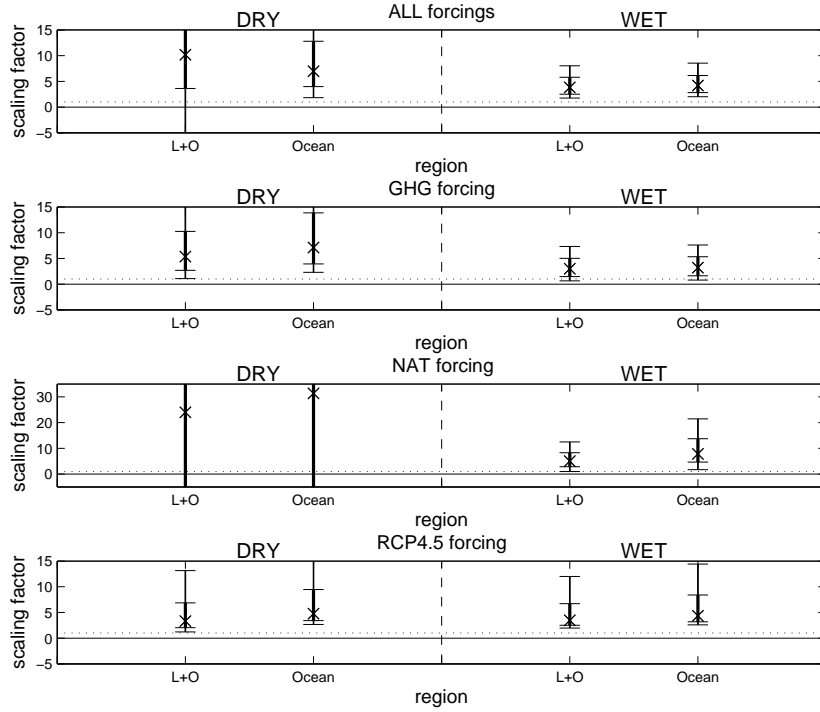


FIG. S19. Detection and attribution results: As Figure 3 upper panel but using fingerprints for individual forcings and wet and dry regions separately. Scaling factor for the ALL, GHG, NAT, and RCP4.5 simulations for wet and dry regions separately with ENSO removed from observations. Crosses show the 'best-guess' scaling factor for the multi-model mean, thick lines are the 90% confidence interval for the raw model variance added as noise and thin lines are the 90% confidence interval for double the variance. Note different scale used for NAT forcing. The residual consistency test is passed for all forcings for double the model variance.

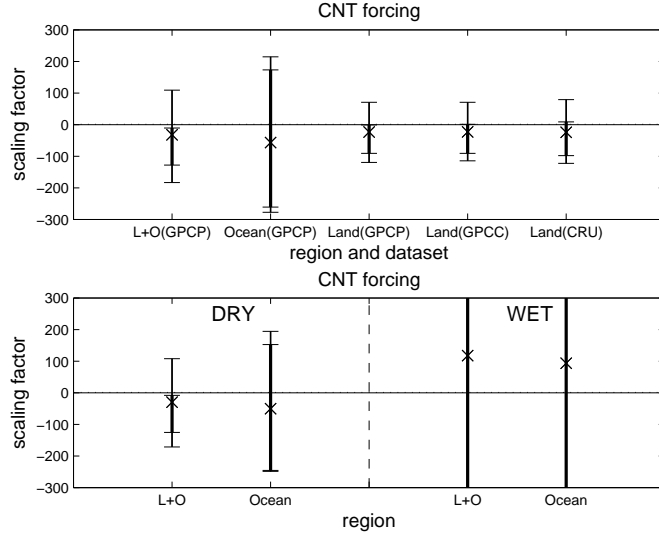


FIG. S20. Detection and attribution results: As Figure 3 upper panel but using fingerprints for control only simulations. UPPER PANEL Scaling factors for the control simulations fingerprint for combined dry and wet regions for land+ocean, ocean only and land only for the 3 observations datasets GPCP, GPCC and CRU and LOWER PANEL individual dry and wet regions for land+ocean for the GPCP dataset. This shows that no artificial trends are introduced by the analysis method that produce false detection if forcing.